www.czasopisma.pan.pl PAN POLSKA AKADEMIA NAUK www.journals.pan.pl

A R C H I V E S O F M E T A L L U R G Y A N D M A T E R I A L S

Volume 60 2015 Issue 2

DOI: 10.1515/amm-2015-0215

T. SKRZYPCZAK*,♯, E. WĘGRZYN-SKRZYPCZAK**, J. WINCZEK*

EFFECT OF NATURAL CONVECTION ON DIRECTIONAL SOLIDIFICATION OF PURE METAL

WPŁYW KONWEKCJI SWOBODNEJ NA KRZEPNIĘCIE KIERUNKOWE CZYSTEGO METALU

The paper is focused on the modeling of the directional solidification process of pure metal. During the process the solidification front is sharp in the shape of the surface separating liquid from solid in three dimensional space or a curve in 2D. The position and shape of the solid-liquid interface change according to time. The local velocity of the interface depends on the values of heat fluxes on the solid and liquid sides. Sharp interface solidification belongs to the phase transition problems which occur due to temperature changes, pressure, etc. Transition from one state to another is discontinuous from the mathematical point of view. Such process can be identified during water freezing, evaporation, melting and solidification of metals and alloys, etc.

The influence of natural convection on the temperature distribution and the solid-liquid interface motion during solidification of pure copper is studied. The mathematical model of the process is based on the differential equations of heat transfer with convection, Navier-Stokes equation and the motion of the interface. This system of equations is supplemented by the appropriate initial and boundary conditions. In addition the continuity conditions at the solidification interface must be properly formulated. The solution involves the determination of the temporary temperature and velocity fields and the position of the interface. Typically, it is impossible to obtain the exact solution of such problem. The numerical model of solidification of pure copper in a closed cavity is presented, the influence of the natural convection on the phase change is investigated. Mathematical formulation of the problem is based on the Stefan problem with moving internal boundaries. The equations are spatially discretized with the use of fixed grid by means of the Finite Element Method (FEM). Front advancing technique uses the Level Set Method (LSM). Chorin's projection method is used to solve Navier-Stokes equation. Such approach makes possible to uncouple velocities and pressure. The Petrov-Galerkin formulation is employed to stabilize numerical solutions of the equations. The results of numerical simulations in the 2D region are discussed and compared to the results obtained from the simulation where movement of the liquid phase was neglected.

Keywords: Pure Metal, Solidification, Sharp Interface, Natural Convection, Finite Element Method, Level Set Method

Praca porusza problematykę modelowania kierunkowego krzepnięcia czystego metalu. Podczas tego procesu obserwuje się formowanie ostrego frontu krzepnięcia w postaci powierzchni separującej ciecz i ciało stałe w przypadku trójwymiarowym lub krzywej w przypadku płaskim. Położenie oraz kształt interfejsu krzepnięcia zmieniają się w czasie a wartości prędkości lokalnych zależą od różnicy intensywności strumieni ciepła po stronie ciała stałego i cieczy. Krzepnięcie z ostrym frontem należy do grupy procesów z przemianami fazowymi, które warunkowane są zmianami temperatury, ciśnienia, itp. Przejście fazowe z jednego stanu w drugi ma z matematycznego punktu widzenia charakter nieciągły. Procesy tego typu można zidentyfikować podczas zamarzania wody, parowania, topnienia i krzepnięcia metali i stopów, itp. W pracy zbadano wpływ zjawiska konwekcji swobodnej na chwilowy rozkład temperatury oraz ruch granicy narastania fazy stałej podczas krzepnięcia czystej miedzi w obszarze płaskim. Model matematyczny sformułowano na bazie równań różniczkowych transportu ciepła z konwekcją, Naviera-Stokesa i ruchu frontu krzepnięcia. Układ równań uzupełniono odpowiednimi warunkami początkowymi i brzegowymi oraz warunkami ciągłości na froncie. Rozwiązanie obejmuje chwilowe rozkłady temperatury, prędkości oraz położenie granicy międzyfazowej. Sformułowanie matematyczne zagadnienia bazuje na modelu z ruchomymi granicami wewnętrznymi, czyli tzw. modelu Stefana. Równania zostały zdyskretyzowane przestrzennie z wykorzystaniem metody elementów skończonych. W modelu numerycznym wykorzystano siatkę niezmienną w czasie. Do propagacji frontu użyto metody poziomic. Do wyznaczenia prędkości w cieczy wykorzystano metodę rzutowania, która poprzez eliminację ciśnienia z równania pędu pozwala na rozprzężenie prędkości i ciśnień. Równania rozwiązano z wykorzystaniem sformułowania Petrova-Galerkina. Omówiono wyniki analizy numerycznej oraz porównano je z wynikami otrzymanymi z symulacji, w której pominięto ruch cieczy.

* INSTITUTE OF MECHANICS AND MACHINE DESIGN FUNDAMENTALS, FACULTY OF MECHANICAL ENGINEERING AND COMPUTER SCIENCE, CZESTOCHOWA UNIVERSITY OF TECHNOLOGY, 69 DĄBROWSKIEGO STR., 42-201 CZĘSTOCHOWA, POLAND

** INSTITUTE OF MATHEMATICS, FACULTY OF MECHANICAL ENGINEERING AND COMPUTER SCIENCE, CZESTOCHOWA UNIVERSITY OF TECHNOLOGY, 69 DĄBROWSKIEGO STR., 42-201 CZĘSTOCHOWA, POLAND

♯ Corresponding author: skrzyp@imipkm.pcz.pl

1. Introduction

In the case of alloy solidification front is usually unstable. This phenomenon is caused by the segregation of the alloy components at the front and is called solutal undercooling [1-3]. It leads to the formation of a region filled with the solid-liquid mixture called mushy zone. If the explicit effect of component segregation is neglected one can consider it indirectly using one of the models involving solidification between the solidus and liquidus temperatures. They are widely used to model various technological processes containing solidification such as continuous casting or welding [4-10].

Morphology of the solid-liquid interface during solidification process of pure metals depends on the direction of heat flow [2]. In equiaxed solidification front is morphologically unstable because the grains grow into an undercooled liquid. Perturbation which forms on the edge of the grain has favorable thermal conditions to grow. During directional solidification the direction of solid phase growth is opposite to that of heat flow. When a perturbation appears at a smooth interface it melts back and the planar interface remains smooth. As a result, the solid-liquid interface during directional solidification of a pure substance is always stable.

The main problem in modeling directional solidification process of a pure material is the appropriate mathematical and numerical descriptions of the motion of the interface. Both heat diffusion, caused by heat transfer between the atoms and convection, caused by the movement of the liquid phase have an influence on the shape and temporary position of the solidification front. If the fluid flow is driven by the differences in the fluid density due to the vertical temperature gradient then it is called the natural convection. Forced convection occurs when the motion is induced by external influences, such as pumps, fans, etc. Despite its importance in many industrial applications, melting or solidification of metals with natural convection in the liquid phase has received only little research attention. Experiments with lead in 1970 [11], mercury in 1974 [12], gallium in 1986 [13], and tin in 1987 [14] have demonstrated, however, that natural convection can significantly affect the shape of solidification interface. This has also been confirmed by numerical studies of melting of pure metals in 1986 [15] and 1987 [14]. Numerical investigations of the pure metal solidification with convection were also carried out in 90's [16, 17] and in the recent years [18, 19].

Mathematical description of the motion of the solidification interface in the case of pure metal is based on the Stefan conditions on the moving internal boundary. These conditions make possible to estimate the local velocity of the interface. The velocity can be used in the appropriate differential equation to track the interface according to time. Interface tracking algorithms are usually based on the phase-field method [20-22], cellular automata [23] or the Level Set Method [24-28]. The main idea of the phase-field method is to introduce a phase-field variable that varies smoothly from zero to unity between the solid and liquid phases over the region, which is narrow but it has numerically resolvable thickness. LSM is an alternative method to track the sharp interface directly. It is widely used in various applications such as solidification of pure substances, dendritic growth, two-phase flows, crack propagation, image processing. In this method, interfacial geometric quantities such as curvature and outward normal can be estimated with the use of level set field φ. The method was first applied to Stefan problems in [29].

Computer simulations of the sharp front solidification processes is a challenge for developers of specialized software especially in the case of complex geometries and non-connected, curved interfaces. Important requirement of the software is to obtain very good accuracy of the temperature distribution on both sides of the moving front which can be arbitrarily located between the nodes of the finite element mesh. It leads to considerable difficulties in determining the temperature in its vicinity. There are various methods to resolve this problem which can be divided into three groups:

- methods using modifications of approximation functions in the finite elements containing solidification interface. In this case the finite element mesh does not change according to time [30];
- methods using mesh adaptation where the edges of the finite elements are systematically adjusted to the shape of the front [31];
- methods based on the diffused front where solidification at a constant temperature is replaced by the process within a narrow temperature range [32, 33].

2. Mathematical model

Process of directional solidification of pure metal with natural convection of the liquid phase is taken into account. Scheme of the process is shown in Fig. 1. Solid Ω_L and liquid Ω_S regions are separated by the solidification front Γ_{LS} which changes its position according to time. Heat is transported in the direction of the solid. It has stabilizing impact on the shape of Γ_{LS}. The rate of growth of the solid has a direct influence on the position of Γ_{LS}. Differences in temperature field in the vertical direction cause the movement of the liquid metal due to density changes. Zero contour line of the level set field φ denotes temporary position of the interface Γ_{LS}.

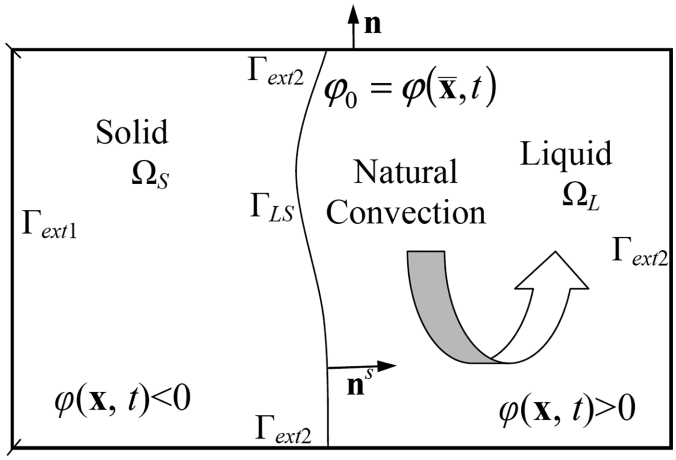

Fig. 1. Scheme of the directional solidification of pure metal with natural convection

The mathematical model of analyzed process contains following differential equations:

Heat diffusion-convection equation:

$$\frac{\partial}{\partial x}\left(\lambda\frac{\partial T}{\partial x}\right)+\frac{\partial}{\partial y}\left(\lambda\frac{\partial T}{\partial y}\right)-c\rho\left(u_x\frac{\partial T}{\partial x}+u_y\frac{\partial T}{\partial y}\right)-c\rho\frac{\partial T}{\partial t}=0 \quad (1)$$

where T is the temperature [K], λ – coefficient of thermal conductivity [J s^{-1} m^{-1} K^{-1}], c – specific heat [J kg^{-1} K^{-1}], ρ – density [kg m^{-3}], u_x, u_y – components of the velocity vector [m s^{-1}], t – time [s], x, y – Cartesian coordinates [m].

Navier-Stokes equations in the case of non-isothermal, incompressible flow of a Newtonian fluid:

$$\begin{aligned}\frac{1}{\rho}\left[\frac{\partial}{\partial x}\left(\mu\frac{\partial u_x}{\partial x}\right)+\frac{\partial}{\partial y}\left(\mu\frac{\partial u_x}{\partial y}\right)\right]-\left(u_x\frac{\partial u_x}{\partial x}+u_y\frac{\partial u_x}{\partial y}\right)-\\ \frac{1}{\rho}\frac{\partial p}{\partial x}-g_x\beta(T-T_{ref})=\frac{\partial u_x}{\partial t}\\ \frac{1}{\rho}\left[\frac{\partial}{\partial x}\left(\mu\frac{\partial u_y}{\partial x}\right)+\frac{\partial}{\partial y}\left(\mu\frac{\partial u_y}{\partial y}\right)\right]-\left(u_x\frac{\partial u_y}{\partial x}+u_y\frac{\partial u_y}{\partial y}\right)-\\ \frac{1}{\rho}\frac{\partial p}{\partial y}-g_y\beta(T-T_{ref})=\frac{\partial u_y}{\partial t}\end{aligned} \quad (2)$$

where μ is dynamical viscosity [kg m^{-1} s^{-1}], p – pressure [Pa], β – volumetric coefficient of thermal expansion [K^{-1}], T_{ref} – reference temperature [K], g_x, g_y – components of gravitational acceleration vector [m s^{-2}].

Continuity equation under the assumption of incompressibility:

$$\frac{\partial u_x}{\partial x}+\frac{\partial u_y}{\partial y}=0 \quad (3)$$

Level set equation:

$$u_x^{\Gamma_{LS}}\frac{\partial\phi}{\partial x}+u_y^{\Gamma_{LS}}\frac{\partial\phi}{\partial y}+\frac{\partial\phi}{\partial t}=0 \quad (4)$$

where φ is the function measuring distance to the interface Γ_{LS} [m], $u_x^{\Gamma_{LS}}, u_y^{\Gamma_{LS}}$ – components of the velocity of Γ_{LS}.

The above set of differential equations (1-4) is supplemented by the appropriate boundary and initial conditions.

Boundary conditions:

$$T|_{\Gamma_{ext1}}=T_b,\quad -\lambda\frac{\partial T}{\partial n}\Big|_{\Gamma_{ext2}}=q \quad (5)$$

$$u_x|_{\Gamma_{ext1}\cup\Gamma_{ext2}}=u_y\big|_{\Gamma_{ext1}\cup\Gamma_{ext2}}=0 \quad (6)$$

where T_b is the given boundary temperature [K], Γ_{ext1} – left external boundary, Γ_{ext2} – right, top and bottom external boundaries, q – heat flux normal to the external boundary Γ_{ext2} [J s^{-1} m^{-2}], n – direction of the vector pointing outwards Γ_{ext2}.

Initial conditions:

$$T|_{t=0}=T_0,\quad \phi|_{t=0}=\phi_0,\quad u_x|_{t=0}=u_y\big|_{t=0}=0 \quad (7)$$

where T_0 is the initial temperature [K] and initial position of the Γ_{LS} is indicated by condition φ_0 =0.

Continuity conditions at the solidification interface must be also fulfilled:

$$\begin{aligned}T^s|_{\Gamma_{LS}}=T^l\big|_{\Gamma_{LS}}=T_M\\ \lambda_s\frac{\partial T^s}{\partial n^s}\Big|_{\Gamma_{LS}}-\lambda_l\frac{\partial T^l}{\partial n^s}\Big|_{\Gamma_{LS}}=\rho_s L\left|\mathbf{u}^{LS}\right|\end{aligned} \quad (8)$$

where n^s is the direction of the vector pointing outwards Γ_{LS}, T_M – melting (solidification) temperature [K], $\mathbf{u}^{LS}$ – velocity of the solidification front, L – latent heat of solidification [J kg^{-1} K^{-1}], s, l – means solid or liquid.

3. Numerical model

According to the weighted residuals method, equation (1) is multiplied by a weight function $w = w(x,y)$ and then integrated over the region $\Omega = \Omega_S \cup \Omega_L$.

$$\iint_\Omega w\left(\frac{\partial}{\partial x}\left(\lambda\frac{\partial T}{\partial x}\right)+\frac{\partial}{\partial y}\left(\lambda\frac{\partial T}{\partial y}\right)-c\rho\left(u_x\frac{\partial T}{\partial x}+u_y\frac{\partial T}{\partial y}\right)-c\rho\frac{\partial T}{\partial t}\right)dxdy=0 \quad (9)$$

Above equation can be written as a sum of following integral terms:

$$\begin{aligned}\iint_\Omega w\left(\frac{\partial}{\partial x}\left(\lambda\frac{\partial T}{\partial x}\right)+\frac{\partial}{\partial y}\left(\lambda\frac{\partial T}{\partial y}\right)\right)dxdy-\\ \iint_\Omega wc\rho\left(u_x\frac{\partial T}{\partial x}+u_y\frac{\partial T}{\partial y}\right)dxdy-\iint_\Omega wc\rho\frac{\partial T}{\partial t}dxdy=0\end{aligned} \quad (10)$$

Green's theorem is used to reduce the order of the diffusion term in above equation:

$$\begin{aligned}\iint_\Omega w\left(\frac{\partial}{\partial x}\left(\lambda\frac{\partial T}{\partial x}\right)+\frac{\partial}{\partial y}\left(\lambda\frac{\partial T}{\partial y}\right)\right)d\Omega=\\ -\lambda\iint_\Omega\left(\frac{\partial w}{\partial x}\frac{\partial T}{\partial x}+\frac{\partial w}{\partial y}\frac{\partial T}{\partial y}\right)dxdy+\lambda\oint_{\Gamma_{ext2}}w\left(\frac{\partial T}{\partial x}n_x+\frac{\partial T}{\partial y}n_y\right)ds\end{aligned} \quad (11)$$

where n_x, n_y are the components of the vector normal to Γ_{ext2}.

This operation leads to the following weak form of (9):

$$\begin{aligned}\iint_\Omega\lambda\left(\frac{\partial w}{\partial x}\frac{\partial T}{\partial x}+\frac{\partial w}{\partial y}\frac{\partial T}{\partial y}\right)dxdy+\\ \iint_\Omega wc\rho\left(u_x\frac{\partial T}{\partial x}+u_y\frac{\partial T}{\partial y}\right)dxdy+\iint_\Omega wc\rho\frac{\partial T}{\partial t}dxdy=\oint_{\Gamma_{ext2}}wqds\end{aligned} \quad (12)$$

Matrix form of equation (12) is derived according to FEM and Petrov-Galerkin formulation, where the weight functions $w(x, y)$ differ from the shape functions $N(x, y)$. The whole region is spatially discretized with the use of triangular mesh. Temperature T, its spatial and time derivatives and velocity components u_x, u_y, are approximated in the finite element with the use of shape functions:

$$T=\sum_{i=1}^{3}N_iT_i=[N]\{T\},\quad \frac{\partial T}{\partial t}=\sum_{i=1}^{3}N_i\frac{\partial T_i}{\partial t}=[N]\left\{\frac{\partial T}{\partial t}\right\} \quad (13)$$

$$u_x=\sum_{i=1}^{3}N_iu_{ix}=[N]\{u_x\},\qquad u_y=\sum_{i=1}^{3}N_iu_{iy}=[N]\{u_y\} \quad (14)$$

$$\frac{\partial T}{\partial x}=\sum_{i=1}^{3}\frac{\partial N_i}{\partial x}T_i=[DN_x]\{T\},\quad \frac{\partial T}{\partial y}=\sum_{i=1}^{3}\frac{\partial N_i}{\partial y}T_i=\left[DN_y\right]\{T\} \quad (15)$$

$$q = \sum_{i=1}^{2} \tilde{N}_i q_i = \left[\tilde{N}\right]\{q\} \tag{16}$$

where $\tilde{N}_i$ are the shape functions assigned to the edge of finite element. Matrices used in (13-16) are defined as follows:

$$[N] = \begin{bmatrix} N_1 & N_2 & N_3 \end{bmatrix}, \quad \left[\tilde{N}\right] = \begin{bmatrix} \tilde{N}_1 & \tilde{N}_2 \end{bmatrix} \tag{17}$$

$$[DN_x] = \begin{bmatrix} \frac{\partial N_1}{\partial x} & \frac{\partial N_2}{\partial x} & \frac{\partial N_3}{\partial x} \end{bmatrix}, \quad \left[DN_y\right] = \begin{bmatrix} \frac{\partial N_1}{\partial y} & \frac{\partial N_2}{\partial y} & \frac{\partial N_3}{\partial y} \end{bmatrix} \tag{18}$$

$$\{T\} = \begin{Bmatrix} T_1 \\ T_2 \\ T_3 \end{Bmatrix}, \quad \left\{\frac{\partial T}{\partial t}\right\} = \begin{Bmatrix} \partial T_1/\partial t \\ \partial T_2/\partial t \\ \partial T_3/\partial t \end{Bmatrix}, \quad \{q\} = \begin{Bmatrix} q_1 \\ q_2 \end{Bmatrix} \tag{19}$$

The mathematical form of i-th weight function in the finite element according to Petrov-Galerkin formulation is as follows:

$$w_i = N_i + \chi \frac{h}{2} \frac{u_x \frac{\partial N_i}{\partial x} + u_y \frac{\partial N_i}{\partial y}}{|\mathbf{u}|} \tag{20}$$

where h is the dimension of the finite element in the direction of velocity vector $\mathbf{u}$ and χ is the parameter calculated in the following way:

$$\chi = ctgh\,(Pe) - \frac{1}{Pe} \tag{21}$$

where Pe is the Peclet number calculated with the use of appropriate material properties:

$$Pe = \frac{c\rho\,|\mathbf{u}|\,h}{2\lambda} \tag{22}$$

Weight functions (20) and its spatial derivatives can be stored in the following vectors

$$[W] = \begin{bmatrix} w_1 & w_2 & w_3 \end{bmatrix}, \quad [DW_x] = \begin{bmatrix} \frac{\partial w_1}{\partial x} & \frac{\partial w_2}{\partial x} & \frac{\partial w_3}{\partial x} \end{bmatrix}, \quad \left[DW_y\right] = \begin{bmatrix} \frac{\partial w_1}{\partial y} & \frac{\partial w_2}{\partial y} & \frac{\partial w_3}{\partial y} \end{bmatrix} \tag{23}$$

Relations (13-19) and (23) are used in (12) leading to the following equations for a single finite element:

$$\begin{aligned} &\lambda^{(e)} \iint_{\Omega^{(e)}} \left([DW_x]^T [DN_x] + \left[DW_y\right]^T \left[DN_y\right]\right) dxdy\,\{T\} + \\ &(c\rho)^{(e)} \iint_{\Omega^{(e)}} [W]^T [N]\, dxdy \left\{\frac{\partial T}{\partial t}\right\} + \\ &+ (c\rho)^{(e)} \iint_{\Omega^{(e)}} [W]^T \left(u_x [DN_x] + u_y \left[DN_y\right]\right) dxdy\,\{T\} = \\ &\oint_{\Gamma^{(e)}_{ext2}} \left[\tilde{N}\right]^T \left[\tilde{N}\right] ds\,\{q\} \end{aligned} \tag{24}$$

There are matrices in the above equation that can be written as

$$\mathbf{K}_T^{(e)} = \lambda^{(e)} \iint_{\Omega^{(e)}} \left([DW_x]^T [DN_x] + \left[DW_y\right]^T \left[DN_y\right]\right) dxdy \tag{25}$$

$$\mathbf{A}_T^{(e)} = (c\rho)^{(e)} \iint_{\Omega^{(e)}} [W]^T \left(u_x [DN_x] + u_y \left[DN_y\right]\right) dxdy \tag{26}$$

$$\mathbf{M}_T^{(e)} = (c\rho)^{(e)} \iint_{\Omega^{(e)}} [W]^T [N]\, dxdy \tag{27}$$

$$\mathbf{B}_T^{(e)} = \oint_{\Gamma^{(e)}_{ext2}} \left[\tilde{N}\right]^T \left[\tilde{N}\right] ds\,\{q\} \tag{28}$$

$$\mathbf{T}^{(e)} = \{T\}, \quad \dot{\mathbf{T}}^{(e)} = \left\{\frac{\partial T}{\partial t}\right\} \tag{29}$$

where $\mathbf{K}_T^{(e)}$ is the thermal conductivity matrix, $\mathbf{A}_T^{(e)}$ – heat convection matrix, $\mathbf{M}_T^{(e)}$ – heat capacity matrix, $\mathbf{B}_T^{(e)}$ – vector associated with the boundary conditions.

Substituting (25-29) into (24) leads to the following equation

$$\left(\mathbf{K}_T^{(e)} + \mathbf{A}_T^{(e)}\right)\mathbf{T}^{(e)} + \mathbf{M}_T^{(e)}\dot{\mathbf{T}}^{(e)} = \mathbf{B}_T^{(e)} \tag{30}$$

Time discretization procedure is based on the forward Euler method. Time derivative of T in the range $\Delta t = t^{f+1} - t^f$ is approximated using the scheme as showed

$$t \in \left[t^f, t^{f+1}\right] : \dot{\mathbf{T}} = \frac{\mathbf{T}^{f+1} - \mathbf{T}^f}{\Delta t} \tag{31}$$

Above scheme is substituted into (30) to obtain the following global FEM equation

$$\mathbf{T}^{f+1} = \Delta t \mathbf{M}_T^{-1} \left[\mathbf{B}_T + \left(\frac{1}{\Delta t}\mathbf{M}_T - \mathbf{K}_T - \mathbf{A}_T\right)\mathbf{T}^f\right] \tag{32}$$

Main problem in numerical solution of Navier-Stokes equation is the pressure gradient term which makes global coefficient matrix singular in the case of incompressibility. One of the most popular methods used to obtain numerical solution of N-S equation is the method developed by Chorin in 1968 [34]. According to the projection method the components of the auxiliary velocity $\mathbf{u}^* = \left[u_x^*, u_y^*\right]$ are explicitly computed using equations (2) without the pressure gradient term:

$$\begin{aligned} &\frac{u_x^* - u_x^f}{\Delta t} = \frac{1}{\rho}\left[\frac{\partial}{\partial x}\left(\mu\frac{\partial u_x^f}{\partial x}\right) + \frac{\partial}{\partial y}\left(\mu\frac{\partial u_x^f}{\partial y}\right)\right] - \\ &\left(u_x^f\frac{\partial u_x^f}{\partial x} + u_y^f\frac{\partial u_x^f}{\partial y}\right) - g_x\beta(T - T_{ref}) \\ &\frac{u_y^* - u_y^f}{\Delta t} = \frac{1}{\rho}\left[\frac{\partial}{\partial x}\left(\mu\frac{\partial u_y^f}{\partial x}\right) + \frac{\partial}{\partial y}\left(\mu\frac{\partial u_y^f}{\partial y}\right)\right] - \\ &\left(u_x^f\frac{\partial u_y^f}{\partial x} + u_y^f\frac{\partial u_y^f}{\partial y}\right) - g_y\beta(T - T_{ref}) \end{aligned} \tag{33}$$

where f denotes f-th time level. Further operations will be performed on the equations in the vector form. In the projection step one can obtain

$$\frac{\mathbf{u}^{f+1} - \mathbf{u}^*}{\Delta t} = -\frac{1}{\rho}\nabla p^{f+1} \tag{34}$$

By rewriting (34) for the $\mathbf{u}^{f+1}$ the following equation is obtained

$$\mathbf{u}^{f+1} = \mathbf{u}^* - \frac{\Delta t}{\rho}\nabla p^{f+1} \tag{35}$$

By taking the divergence of (35) one can obtain

$$\nabla \cdot \mathbf{u}^{f+1} = \nabla \cdot \mathbf{u}^{*} - \frac{\Delta t}{\rho} \nabla^2 p^{f+1} \tag{36}$$

By requiring that $\nabla \cdot \mathbf{u}^{f+1} = 0$ (continuity condition) equation (36) takes the following form

$$\nabla^2 p^{f+1} = \frac{\rho}{\Delta t} \nabla \cdot \mathbf{u}^{*} \tag{37}$$

In conclusion, Chorin's projection method consists of the three steps. Firstly, equations (33) are solved explicitly with the use of Petrov-Galerkin formulation to obtain the auxiliary velocity field $\mathbf{u}^{*} = \left[u_x^{*}, u_y^{*}\right]$. This process is analogous to that presented in the case of equation (1). The local matrices are shown below:

$$\mathbf{K}_u^{(e)} = \left(\frac{\mu}{\rho}\right)^{(e)} \iint_{\Omega^{(e)}} \left([DW_x]^T [DN_x] + \left[DW_y\right]^T \left[DN_y\right] \right) dxdy \tag{38}$$

$$\mathbf{A}_u^{(e)} = \iint_{\Omega^{(e)}} [W]^T \left(u_x^f [DN_x] + u_y^f \left[DN_y\right] \right) dxdy \tag{39}$$

$$\mathbf{M}_u^{(e)} = \iint_{\Omega^{(e)}} [W]^T [N] \, dxdy \tag{40}$$

$$\begin{aligned} \mathbf{B}_{ux}^{(e)} &= \iint_{\Omega^{(e)}} [W]^T [N] \, dxdy \left\{ g_x \beta \left(T - T_{ref} \right) \right\} \\ \mathbf{B}_{uy}^{(e)} &= \iint_{\Omega^{(e)}} [W]^T [N] \, dxdy \left\{ g_y \beta \left(T - T_{ref} \right) \right\} \end{aligned} \tag{41}$$

Aggregation process leads to the global FEM equations:

$$\begin{aligned} \mathbf{u}_x^{*} &= \Delta t \mathbf{M}_u^{-1} \left[\mathbf{B}_{ux} + \left(\frac{1}{\Delta t} \mathbf{M}_u - \mathbf{K}_u - \mathbf{A}_u \right) \mathbf{u}_x^f \right] \\ \mathbf{u}_y^{*} &= \Delta t \mathbf{M}_u^{-1} \left[\mathbf{B}_{uy} + \left(\frac{1}{\Delta t} \mathbf{M}_u - \mathbf{K}_u - \mathbf{A}_u \right) \mathbf{u}_y^f \right] \end{aligned} \tag{42}$$

In the second step Poisson's equation (37) is solved using standard Galerkin formulation to obtain pressure field p^{f+1}. In the third step the solution of the equation (35) gives the real velocity field $\mathbf{u}^{f+1}$.

The numerical treatment of the equation (4) was discussed in details in [35, 36]. The reinitialization of the level set function as well as the calculation of the heat fluxes on the solid and liquid sides of Γ_{LS} were the same as in [36].

4. Examples of calculation

The calculations were performed to show the effect of natural convection of the liquid copper on the temporary position and shape of solidification front. They were carried out in the simple, rectangular geometry with the boundary and initial conditions showed in Fig. 2. Finite element mesh was composed of 95106 triangles with 47952 nodes. At the time t =0 s the initial temperature of the entire region was higher than the melting point of copper and equal to 1500 K. At the left wall Dirichlet boundary condition was used with T_b =300 K. At the other boundaries thermal insulation was employed. Liquid material was motionless at the initial time of the process.

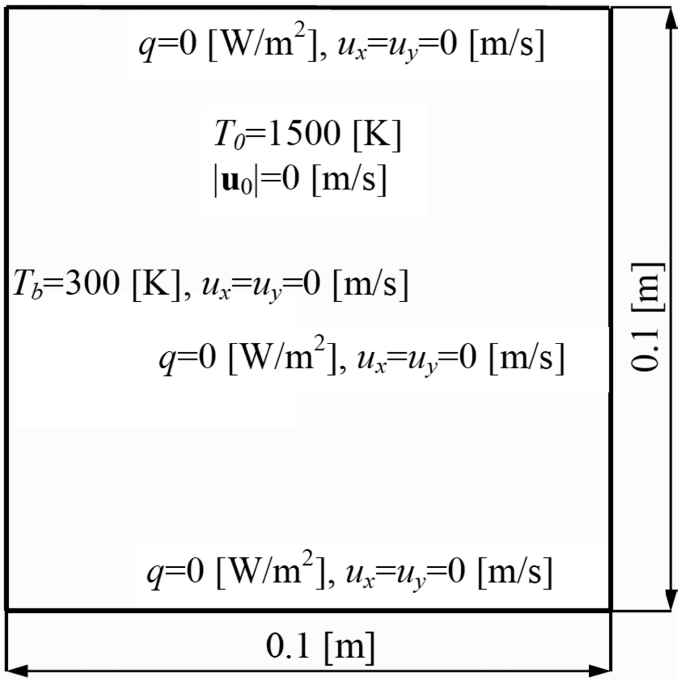

Fig. 2. Geometry of the solidifying region with boundary and initial conditions

Two numerical simulations were performed, the first where the effect of natural convection was included and the second neglecting this phenomenon. The material properties used in both simulations are compiled in Table 1. The main purpose of such approach was to show the differences in numerical results caused by the motion of liquid metal. The time step was equal to 0.00025 s during both simulations.

TABLE 1

Material properties of pure copper [37, 38]

Material property	Solid	Liquid
ρ [kg m^{-3}]	8920.0	8300.0
λ [J s^{-1} m^{-1} K^{-1}]	330.0	250.0
c [J kg^{-1} K^{-1}]	420.0	544.0
μ [kg m^{-1} s^{-1}]	-	0.0035
β [K^{-1}]	-	0.0001
L [J kg^{-1}]	204000.0	
T_M [K]	1357.0	

The results of numerical simulations included temporary distributions of the temperature as well as the velocity fields in the case of natural convection. Temperature and velocity distribution at t =5, 10, 20, 40 s are shown in Fig. 3. Position of the melting point isotherm T_M =1357 K is marked by the dashed curve. Steep temperature gradient appearing on the solid side of the front is clearly noticeable at the very early stage of the process causing the high speed of solid phase growth. Highest velocity rates are noticed after 5 s then they gradually decrease to 0.01 m s^{-1} after 40 s. Velocity vectors form few

closed structures called ”convection cells” especially in the middle of the simulation. Solidification process ended after 55 s. Heat transport in the liquid region taking into account the convection is more efficient than in the case neglecting this factor.

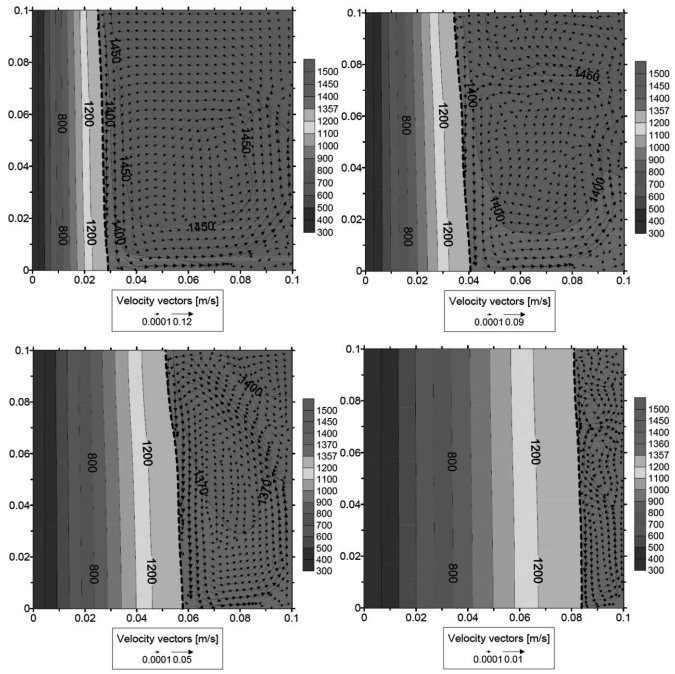

Fig. 3. Temperature and velocity fields after t =5, 10, 20, 40 s

Comparison of the cooling curves at selected nodes is shown in Fig. 4. Temperature in these points decreases more rapidly when they are in the liquid state in the case of natural convection. Differences grow as the distance from the cold wall increases. Melting point is reached a bit earlier than in the case of pure heat diffusion so the duration of the solidification process is a bit shorter if the motion of the liquid phase is included in the model.

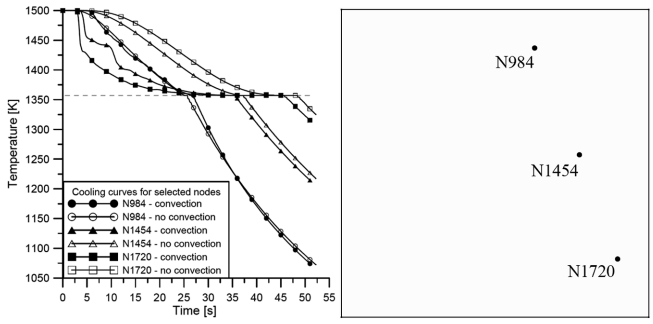

Fig. 4. Comparison of the cooling curves at selected nodes

Temporary positions of the solidification interface obtained from the both cases of simulation are shown in Fig. 5. The comparison was done at selected moments t =2, 5, 10, 20, 30, 40, 50 s. It shows that the differences between locations of the front at the very early stage of the processes are negligible due to very high temperature gradient in the solid region. They are more noticeable as the distance of the solidification front from the cold wall increases. Interface has a shape of a vertical line if the motion of the liquid is neglected but it deforms slightly when the convection is included. This is clearly noticeable as the process evolves.

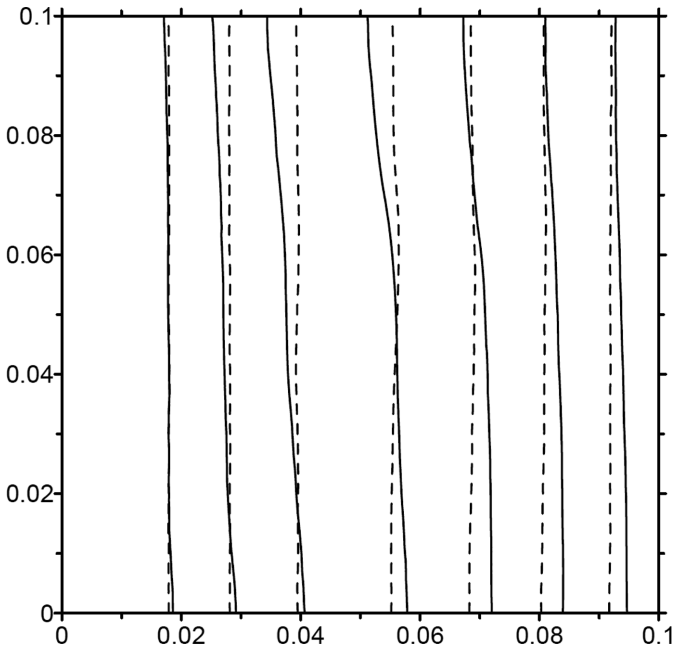

Fig. 5. Comparison of the temporary front positions

The velocity of the solidification front decreases rapidly according to time. The process ended after 55 s in the case of convection and a few seconds later in the case of pure heat diffusion. This shows that the impact of the motion of the liquid on the duration of the solidification in the analyzed case is rather slight.

5. Conclusions

The presented mathematical and numerical models of directional solidification process of pure metal makes possible to take into account the continuity conditions at the sharp solidification interface as well as the natural convection phenomenon. Numerical formulation, based on the finite element method provides a solid base to build the in-home computer program. The comparison of the results obtained with the use of 2D solver shows quite similar final effect of solidification process. The most significant differences are observed during analysis of cooling curves built for selected points. These differences were caused by the more intense rate of heat transfer in the liquid region in the presence of the movement of molten metal. The comparison of the temporary front position shows very subtle differences, especially in a later stage of the process.

REFERENCES

[1] B. Chalmers, Principles of solidification, New York 1964.
[2] W. Kurz, D.J. Fisher, Fundamentals of solidification, Switzerland 1998.
[3] S. Chakraborty, P. Dutta, Int J Numer Meth Fl. **38**, 895-917 (2002).
[4] L. Sowa, A. Bokota, Arch Metall Mater. **57**(4), 1163-1169 (2012).

[5] L. Sowa, Archives of Mechanical Technology and Automation **32**(1), 55-63 (2012).
[6] T. Telejko, Z. Malinowski, M. Rywotycki, Arch Metall Mater. **54**(3), 837-844 (2009).
[7] A. Burbelko, J. Falkus, W. Kapturkiewicz, K. Sołek, P. Drożdż, M. Wróbel, Arch Metall Mater. **57**(1), 379-384 (2012).
[8] W. Piekarska, M. Kubiak, J Therm Anal Calorim. **110**(1), 159-166 (2012).
[9] W. Piekarska, M. Kubiak, Appl Math Model. **37**, 2051-2062 (2013).
[10] W. Piekarska, M. Kubiak, Saternus Z., Arch Metall Mater. **57**(4), 1219-1227 (2012).
[11] J. Szekely, P.S. Chhabra, Metall Trans B. **1B**, 1195-1203 (1970).
[12] F.M. Chiesa, R.I.L. Guthrie, J Heat Trans-T ASME **95**, 377-390 (1974).
[13] C. Gau, R. Viskanta, J Heat Trans-T ASME **108**, 174-181 (1986).
[14] F. Wolff, R. Viskanta, Exp Heat Transfer **1**, 17-30 (1987).
[15] B.W. Webb, R. Viskanta, Numer Heat Transfer **5**, 539-558 (1986).
[16] Y. Chen, Y.-T. Im, J. Yoo, J Mater Process Tech. **52**(2-4), 592-609 (1995).
[17] M. Giangi, F. Stella, Int J Comput Fluid D. **11**(3-4), 341-349 (1999).
[18] G. Kosec, B. Šarler, Mater Sci Forum **649**, 205-210 (2010).
[19] X. Wang, Y. Fautrelle, Int J Heat Mass Tran. **52**(23-24), 5624-5633 (2009).
[20] W. J. Boettinger, J. A. Warren, C. Beckermann, A. Karma, Ann Rev Mater Res. **32**, 163-194 (2002).
[21] A. Karma, W.J. Rappel, Phys Rev E **57**, 4323-4349 (1998).
[22] D.M. Anderson, G.B. McFadden, A.A. Wheeler, Physica D **135**, 175-194 (2000).
[23] D. Gurgul, A. Burbelko, Arch Metall Mater. **55**(1), 53-60 (2010).
[24] D. Adalsteinsson, J. A. Sethian, J Comput Phys. **118**, 269-277 (1995).
[25] T. Barth, J. Sethian, J Comput Phys. **145**, 1-40 (1998).
[26] S. Osher, J. A. Sethian, J Comput Phys. **79**, 12-49 (1988).
[27] D. Peng, B. Merriman, S. Osher, H. Zhao, J Comput Phys. **155**, 410-438 (1999).
[28] M. Sussman, E. Fatemi, J Sci Comput **20**, 1165-1191 (1999).
[29] S. Chen, B. Merriman, S. Osher, P. Smereka, J Comput Phys. **135**, 8-29 (1997).
[30] J. Chessa, P. Smolinski, T. Belytschko, Int J Numer Meth Eng. **53**, 1959-1977 (2002).
[31] G. Bell, Int J Heat Mass Tran. **21**, 1357-1362 (1986).
[32] G. Comini, S. D. Guidice, R. W. Lewis, O. C. Zienkiewicz, Int J Numer Meth Eng. **8**, 613-624 (1974).
[33] D. Rolph III, K.J. Bathe, Int J Numer Meth Eng. **18**, 119-134 (1982).
[34] A.J. Chorin, Math Comput. **22**, 746-762 (1968).
[35] T. Skrzypczak, E. Węgrzyn-Skrzypczak, Int J Heat Mass Tran. **55**, 4276-4284 (2012).
[36] T. Skrzypczak, Arch Metall Mater. **57**(4), 1189-1199 (2012).
[37] B. Mochnacki, J.S. Suchy, Modelowanie i symulacja krzepnięcia odlewów, Warszawa 1993.
[38] J.A. Cahill, A.D. Kirshenbaum, J Phys Chem-US **66**, 1080-1082 (1962).

Received: 20 April 2014.